Granular temperature profiles in three-dimensional vibrofluidized granular beds

R. D. Wildman,[1] J. M. Huntley,[1] and D. J. Parker[2]
[1]*Wolfson School of Mechanical and Manufacturing Engineering, Loughborough University, Loughborough, Leicestershire LE11 3TU, United Kingdom*
[2]*School of Physics and Astronomy, University of Birmingham, Edgbaston, Birmingham B15 2TT, United Kingdom*
(Received 26 December 2000; published 29 May 2001)

The motion of grains in a three-dimensional vibrofluidized granular bed has been measured using the technique of positron emission particle tracking, to provide three-dimensional packing fraction and granular temperature distributions. The mean square fluctuation velocity about the mean was calculated through analysis of the short time mean squared displacement behavior, allowing measurement of the granular temperature at packing fractions of up to $\eta \sim 0.15$. The scaling relationship between the granular temperature, the number of layers of grains, and the base velocity was determined. Deviations between the observed scaling exponents and those predicted by recent theories are attributed to the influence of dissipative grain-sidewall collisions.

DOI: 10.1103/PhysRevE.63.061311 PACS number(s): 45.70.Mg, 51.10.+y, 05.60.−k

I. INTRODUCTION

The importance of granular materials in industrial and natural processes has led to a long history of study into granular behavior. Over the last 20 years this interest has steadily increased, as the complexity and variety of granular phenomena have become apparent. The similarities between granular materials and classical fluids have been noted frequently (e.g., Ref. [1]). There are, however, fundamental differences between these states of matter; for example, dissipation of kinetic energy during collisions, not observed in simple thermal fluids, is a dominant feature of granular gases. Despite this, the use of kinetic theory analogs has resulted in the first tentative steps towards the construction of a framework in which a hydrodynamic theory of granular flows can be formulated [2].

Much of the progress in understanding granular flows has been through theoretical and numerical approaches (e.g., see Ref. [3]). Recently though, a number of experimental techniques have been developed to investigate two- and three-dimensional vibrofluidized granular beds. In two dimensions, a series of experiments by Warr and co-workers, using high-speed digital photography, demonstrated that highly vibrofluidized two-dimensional (2D) granular beds can operate near to equilibrium, i.e., the granular velocities broadly follow Maxwell distributions [4,5], and that the local structure of the granular bed is similar to that seen in a thermal fluid [6]. Later, a novel method of calculating granular temperature was developed [7] based upon the short-time behavior of the mean squared displacement, which does not require detection of the collision events. This method was used to measure granular temperature concurrently with measurements of the self-diffusion coefficient [8]. This subsequently allowed simple kinetic theory approaches to granular beds to be validated [8].

The visualization of the internal dynamics of three-dimensional granular flows is obviously more challenging than for two-dimensional arrays. A number of techniques have recently been developed to probe flows in three-dimensional geometries, including diffusive wave spectroscopy [9], magnetic resonance imaging [10], and positron emission particle tracking (PEPT) [11]. The authors have recently demonstrated the suitability of PEPT for studies of highly fluidized granular beds [12]. In that article, it was shown that variables such as the mean squared displacement and self-diffusion coefficient could be measured, and that for very dilute systems (packing fractions ~ 0.05) the granular temperature could be measured over the whole altitude range of amplitudes.

In this paper, results from the recently upgraded PEPT facility are presented. The new facility provides an improvement in temporal resolution by a factor of 3–4 compared to the system used in Ref. [12]. As a result granular temperature can be measured in significantly denser flows than was previously possible. In particular, granular temperature profiles will be presented for packing fractions up to about 15% for the first time. An introduction to the PEPT and shaker system is given in Sec. II. In Sec. III, the PEPT location data are analyzed to determine the packing fraction and velocity fields throughout the whole of the cell, and granular temperature profiles for a range of experiments are presented. Finally, scaling laws in three-dimensional fluidized beds are discussed in Sec. IV, where experimentally determined scaling relationships are compared to the two-dimensional experimental results of Warr, Huntley, and Jacques [5], the numerical results of Luding, Herrmann, and Blumen [21], and the theoretical predictions of Kumaran [24].

II. EXPERIMENTAL PROCEDURE

Whole field methods of analyzing highly fluidized three-dimensional granular beds at the single particle level are not generally available. In this paper we present results using the recently upgraded Birmingham PEPT facility. Although PEPT tracks only a single particle, the automated facility allows experimental data to be logged for a considerable length of time (up to 6 h), resulting in pseudo-whole-field data for steady state systems. The technique has recently been used to investigate a number of experimental situations, e.g., rotating beds [13] and paste flow [14] and more recently it has been used to successfully analyze three-dimensional vibrofluidized granular beds [12]. The technique uses a ra-

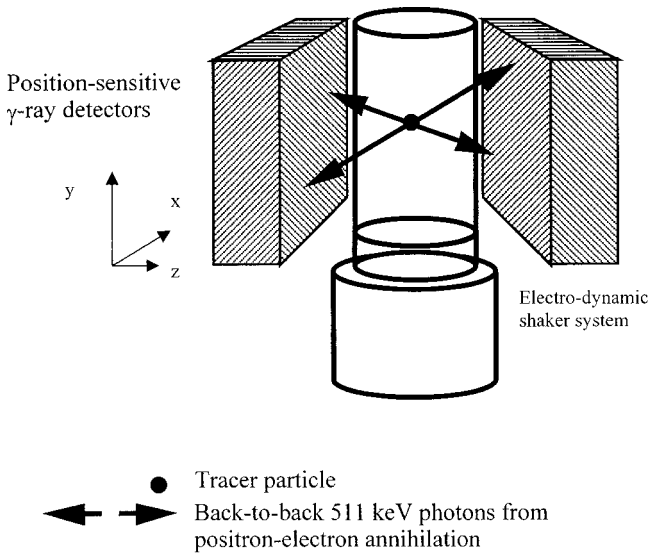

FIG. 1. Schematic of the positron emission particle tracking and shaker facility. The polymethyl methacrylate cylindrical cell was 145 mm in diameter and 300 mm in height.

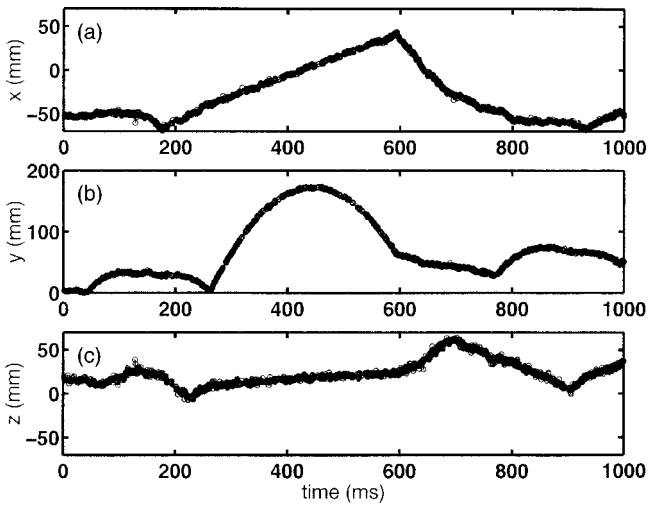

FIG. 2. Typical positron emission particle tracking traces for the (a) x coordinate, (b) y coordinate, and (c) the z coordinate, for $N=350$.

dionuclide that decays by positron emission, and relies on detecting the pairs of back-to-back gamma rays produced when positrons annihilate with electrons. These gamma rays are very penetrating and an accurate location can be determined from detection of a small number of back-to-back pairs. Coincident detection of two gamma rays in a pair of position sensitive detectors defines a line passing close to the point of emission without the need for collimation. The University of Birmingham Positron Camera is a Forte dual headed gamma camera (Adac Laboratories, CA, USA). Each head contains a single crystal of NaI scintillator, 500×400 mm^2, 16 mm thick, optically coupled to an array of photomultiplier tubes. The current maximum count rate of 4×10^4 s^{-1} enables an ideal temporal resolution of 2 ms with a spatial accuracy of ~1 mm. In the following experiments a tracer particle was created by irradiating a glass ballotini sphere with a beam of ^{3}He, which leads to a bead that is physically indistinguishable from the remaining beads within the experimental cell. This radiolabeling process converts the available O nuclei to a radioisotope of F, which decays resulting in the emission of positrons. In a dense medium such as ballotini, a positron quickly annihilates with an electron, producing two back-to-back 511 keV gamma rays. These are detected in the pair of diametrically placed camera heads (Fig. 1). Through triangulation of successive location events, the position of the tracer particle can be located in three dimensions.

A three-dimensional granular gas was generated using a Ling Dynamic Systems (LDS) vibration system. A sinusoidal signal was fed through a field power supply [LDS FPS 1] and power amplifier [LDS PA 1000] into a wide frequency band electrodynamic transducer [LDS V651]. This system has a frequency range of 5–5000 Hz, a maximum acceleration of 100 g and maximum amplitude of 12.5 mm. A cell of dimensions 140 mm diameter and 300 mm height was placed on the upper surface of the vibrating piston, itself placed between the photon detectors (Fig. 1). The cell was constructed of polymethyl methacrylate to limit the attenuation of the gamma rays as they traveled through the experimental apparatus, and the walls were coated with conducting copper tape to reduce electrostatic charging of the grains. The cell was vibrated at a frequency of 50 Hz. The amplitude of vibration, A_O, was varied throughout the range 0.74, 0.94, 1.14, 1.34, and 1.54 mm. Glass ballotini balls of diameter, $d=5.0\pm0.2$ mm (with an intergrain restitution coefficient ε, measured using high-speed photography, of 0.91 and mass, $m=1.875\times10^{-4}$ kg) were used as the granular medium.

At grain speeds of about $\overline{c}=1$ m s^{-1} the PEPT camera has an accuracy, in the x-y plane, of about ±1 mm. However, the accuracy in the z direction is substantially worse as the grain needs to be located in a direction normal to the faces of the detectors. When calculating the granular temperature (Sec. III D), the average behavior in the z direction was therefore assumed to be equivalent to that in the x, due to cylindrical symmetry. During each experiment, the motion of a grain was followed for about 1 h, resulting in up to 20 million location events. Each location event was ascribed a coordinate in space and time (x, y, z, t). The number of grains, N, placed within the cell (including the tracer particle) was chosen to be 350, 700, and 1050 corresponding to a total number of close-packed grain layers of about 0.5, 1, and 1.5, respectively. Figures 2(a)–2(c) show typical x, y, and z trajectories over a 1 s time interval for $N=350$ and $A_O=1.34$ mm.

III. DATA ANALYSIS

A. Center-of-mass motion

In any dissipative system, energy has to be continually injected into the system to maintain the steady state. In the case of vibrofluidized beds, the main energy source is the vibrating lower boundary of the cell. As this motion is confined to the vertical direction, the energy transferred to the grains also flows in the y direction; subsequent intergrain

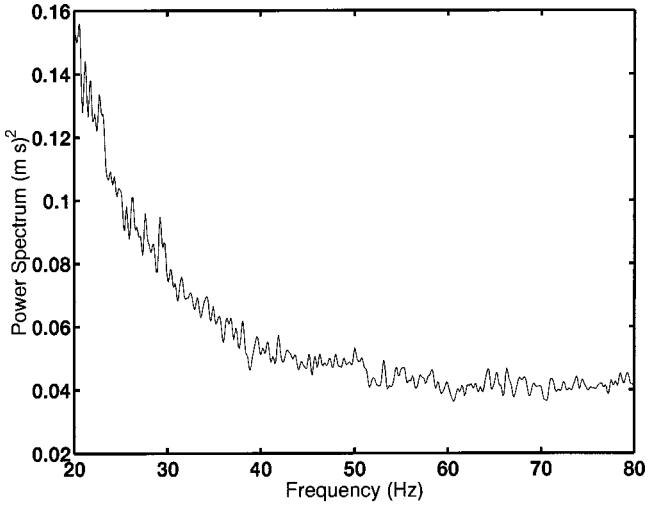

FIG. 3. Average power spectrum of the y coordinates for $N=1050$, $A_O=0.74$ mm.

collisions transfer the kinetic energy into the orthogonal directions, and a form of energy partition occurs [15].

It is well known that sinusoidal excitation can, under certain circumstances (such as low frequency, low ε, and high N), result in significant correlations between the center-of-mass motion of the grains and the motion of the base. Typically, the center of mass moves at some integral fraction of the driving frequency [16]. Granular temperature specifies the magnitude of the velocity fluctuations about the mean flow, and it is therefore important for the calculations in Sec. IV that the center-of-mass motion is determined.

Figure 3 shows part of the frequency spectrum, $P(f)$, defined by

$$P(f)=\left|\sum_{j=1}^{N_j} y_j(t_j)\exp(-i2\pi t_j f)\right|^2, \tag{1}$$

where N_j is the number of coordinate locations, y_j and t_j are the height and time associated with the jth location event, and f is the frequency. $P(f)$ was calculated for the y motion of the tracer particle under conditions potentially most prone to systematic center-of-mass motion ($N=1050$, $A_O=0.74$ mm, for grains in the interval $0<y<5$ mm above the base). The plot in Fig. 3 was obtained by dividing the entire run into sequences lasting 1 s, subtracting the mean y value from each sequence to remove the dc peak from the spectrum, and finally averaging over the resulting 3600 spectra. No significant peak is visible at either 50 Hz, or at any harmonic or subharmonic of this driving frequency. It was therefore assumed that the center-of-mass motion could be disregarded for the range of packing fractions examined in this paper.

B. Packing fraction

In three dimensions, the packing fraction η is defined as

$$\eta=\frac{\text{Volume of particles}}{\text{Total volume}}. \tag{2}$$

During experiments on two-dimensional systems, η can be determined using whole field techniques such as high-speed photography [5]. With a pointwise technique such as PEPT, packing fraction can only be calculated by making use of the ergodicity of the system. This method was developed in a previous publication [12], and will only be described briefly here.

The experimental cell is discretized into segments, the shape of which depends on the analysis being performed. For example, to measure the packing fraction, averaged over the cross-sectional area of the cell, the experimental cell is subdivided into horizontal slices, and packing fraction is calculated as a function of height, y. The large number of location events means that each of these slices can be subdivided further, so that, for example, packing fraction can be measured as a function of r, the distance from the axis, as well as a function of y. Following this segmentation, each location event is assigned to the appropriate segment, resulting in a location density. To accurately determine the packing fraction, the system is assumed to be ergodic [12], i.e., a time average is equivalent to an ensemble average, leading to the expression:

$$\eta=\frac{NF_i(y)\pi d^3}{6V_i}, \tag{3}$$

where V_i is the volume of the ith segment and $F_i(y)$ is distribution of residence times. Figures 4(a)–4(d) show the packing fraction as a function of the altitude, y. Figure 4(a) illustrates the changes in the packing fraction with the number of particles, N, at a fixed amplitude (1.34 mm). The form of the curve is similar in each case: a sharp rise in packing fraction near the base, reaching a peak value and then decaying exponentially. Figure 4(b) demonstrates the influence of the vibration amplitude, for $N=350$, and $A_O=0.74$, 0.94, 1.14, and 1.34 mm. Clearly at low amplitudes the grains are less energetic and accumulate close to the base. At higher amplitudes the base velocity is increased and the bed is expanded. One can see in Fig. 4(c) that a log-linear representation of Fig. 4(b) confirms the tendency of the packing fraction profile to become exponential at high altitudes.

Figure 4(d) shows the packing fraction plotted as a function of the radial distance r for $y=2.5$ to 22.5 mm, and for $N=350$, $A_O=1.34$ mm. There is a significant increase in packing fraction near the wall compared to that on the axis, of around 50% for $y\sim 12.5$ mm. This ''boundary layer'' extends inwards by about 30–40 mm, or about 6–8 grain diameters. The rise in packing fraction could be attributed to a combination of two mechanisms. First, the particles inside the cylindrical cell exert an unbalanced pressure on the grains near the outer surface, pushing the latter towards the wall of the cell [17]. Second, any increase in the packing fraction leads to greater collision rates with the wall. This causes enhanced dissipation, reduced granular temperature, and hence, further increases in density near the wall.

C. Mean velocity fields

Convection in vibrated granular beds is a well-known phenomenon, particularly for low-amplitude regimes. Re-

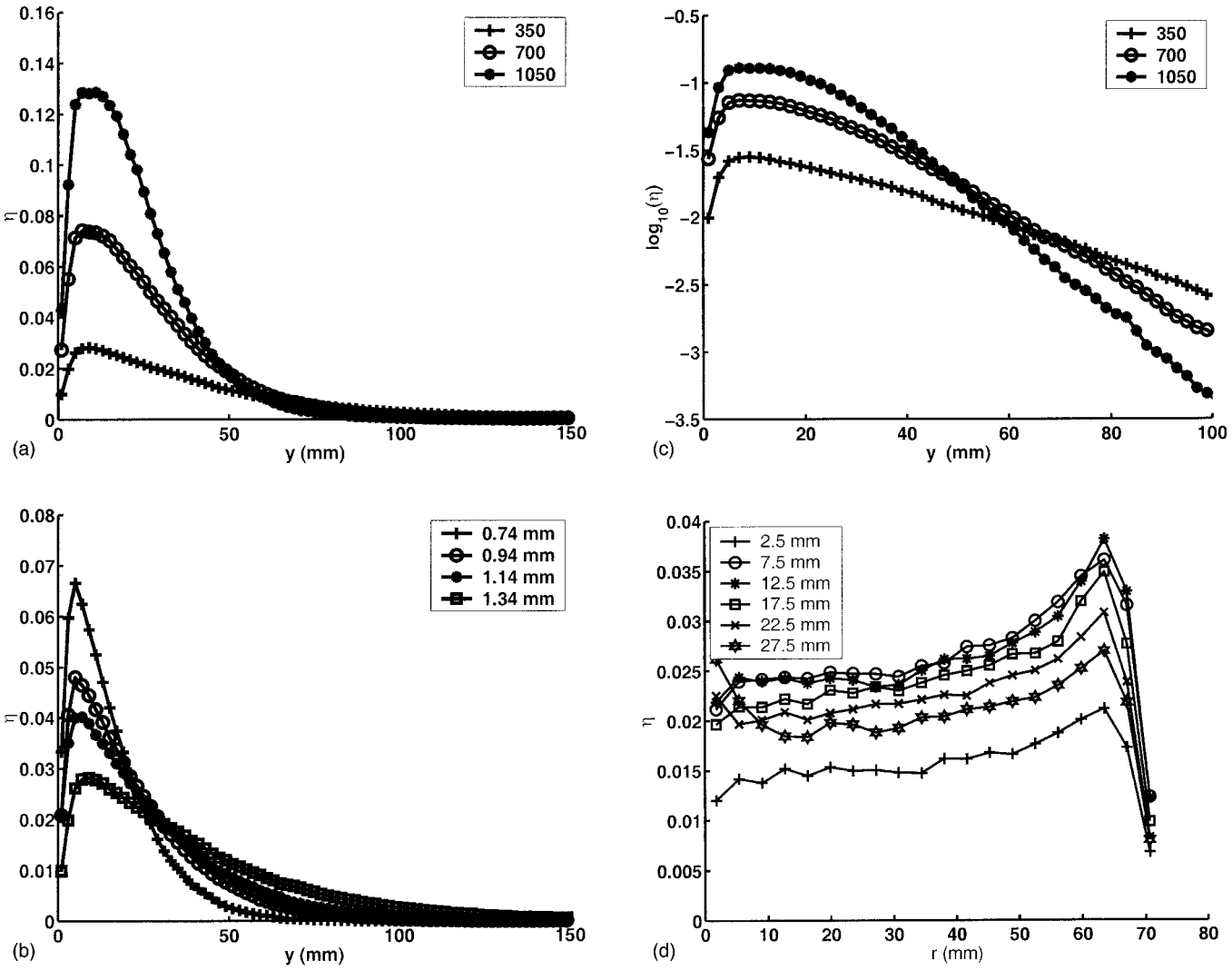

FIG. 4. Packing fraction profiles determined using Eq. (3). (a) Packing fraction vs y for a range of N, $A_O = 1.34$ mm, (b) packing fraction vs y for a range of A_O, $N = 350$, (c) logarithm of packing fraction vs y. $A_O = 1.34$ mm, $N = 350$, 700, and 1050. (d) Packing fraction vs distance from the axis, r, as a function of height, y. $A_O = 1.34$ mm, $N = 350$.

cently this effect has also been observed for the first time in highly fluidized beds [12,18]. In the present paper, our primary interest is in the velocity fluctuations, rather than the mean velocity field, but for completeness we include Fig. 5. This demonstrates that the mean collective speed of the grains is of the order of $\sim 0.05\ \mathrm{m\,s^{-1}}$, and thus that the convection speed is typically less than 10% of the root mean squared velocity. The mean velocity field can thus be neglected as a significant contributory factor in the measurement of granular temperature in most cases explored in this paper.

D. Granular temperature

The similarity of granular flows to thermal fluids has led to the extension of many of the concepts used in the analysis of classical gases and liquids. An analog to the thermodynamic temperature can be defined in terms of the mean kinetic fluctuation energy of the grains,

$$E_O = \tfrac{1}{3} m \overline{c^2}, \tag{4}$$

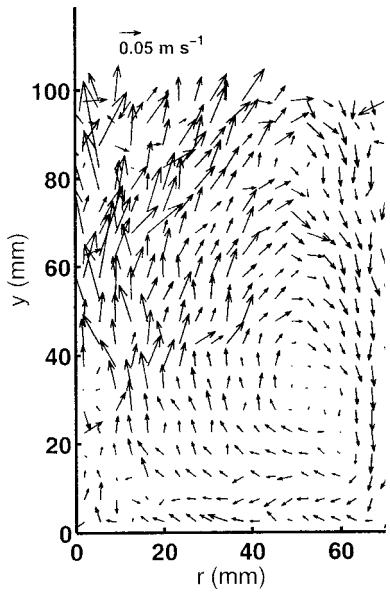

FIG. 5. Mean velocity field for $N = 350$ and $A_O = 1.34$ mm.

where E_O is the granular temperature, m is the mass of a grain, and c is the grain speed. A combination of the dissipation and the vertical motion of the base causes the granular temperature to be anisotropic, which can be characterized by defining granular temperature in each direction:

$$E_i = m\overline{v_i^2}, \tag{5}$$

where i denotes the directions x, y, or z and v is the grain velocity.

Granular temperature is in principle easiest to measure through direct calculation of the second moment of the velocity distribution, or by fitting an expected functional form to the measured velocity distribution [5,7]. Applying these methods to PEPT data presents some difficulties, however, as the collision events are difficult to determine reliably, leading to the likelihood of introducing errors through the averaging of the velocity over collision events. A new method was developed during experiments on two-dimensional systems that allowed both numerical differentiation and collision detection to be avoided, thereby avoiding several significant error sources [7]. This method is dependent on being able to measure the mean squared displacement accurately for times less than or equal to the mean collision time; in two dimensions this procedure was shown to give more reliable data at higher packing fractions than either of the alternatives described above. This approach was applied successfully to 3D PEPT data in Ref. [12] for very dilute cases ($\sim$0.5 layers of beads, giving rise to a peak packing fraction of $\eta \sim 0.05$ and a minimum Enskog mean free time $\tau_E \sim 10$ ms). Improvements in the temporal resolution from $\sim$7 to $\sim$2 ms with the new PEPT system have allowed the number of layers to be increased to $\sim$1.5 for the current set of experiments.

The measurement of the mean squared displacement has been discussed in depth in previous publications and the reader is referred to these for more detail [7,8,12]. Essentially, each location event is considered as the start of an independent trace. Then the grain is followed for 200 ms, the square of the displacement being recorded for every subsequent location event. Once this has been completed for every grain location in each segment, the mean squared displacement is binned according to the time of location, and the ensemble average is calculated. Typical results for this technique are shown in Fig. 6. The mean squared speed, and thus the granular temperature, is extracted from 2nd order polynomial regression applied to the short-time ballistic behavior of the mean squared displacement [7].

Figures 7 and 8 show granular temperature profiles for $N = 1050$ grains for both the x and y directions. These figures clearly show that the granular temperature is anisotropic; granular temperature in the y direction is larger than that in the x. This has been observed consistently in both experimental and numerical studies and, as noted before, is due to energy being injected in the y direction and then being transferred into the x direction through collisions.

For high amplitudes ($A_O > 1.14$ mm) and high N, one observes that the granular temperature appears to increase with altitude. One possible reason for this upturn is the effect of convection. The velocities associated with the mean flow field are relatively low magnitude and were not taken into account in the numerical analysis procedures used to calculate granular temperatures. The effect of ignoring the mean field on the calculated granular temperature can be estimated by assuming that the velocity distribution is Gaussian about a constant convection velocity, v_C, i.e.,

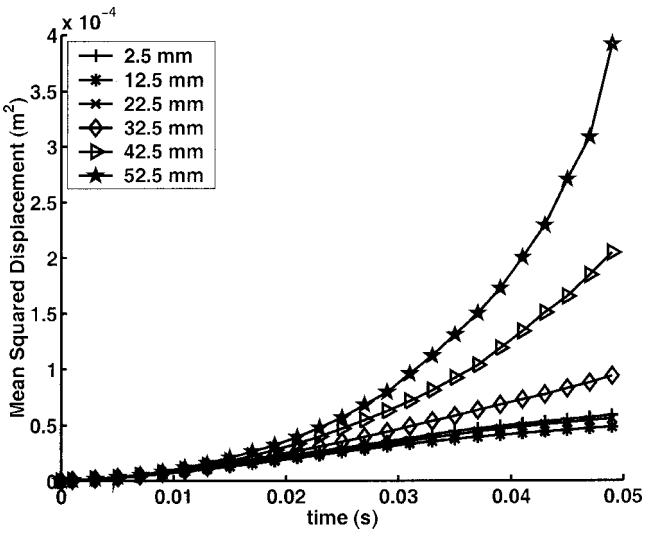

FIG. 6. Mean squared displacement for $N = 350$ and $A_O = 1.34$ mm, as a function of height, y.

$$P[v_Y]dv_Y = \left(\frac{m}{\pi E_Y}\right)^{1/2} \exp\left(-\frac{m(v_Y - v_C)^2}{E_Y}\right) dv_Y. \tag{6}$$

The second moment of this distribution,

$$\overline{v_Y^2} = \int_{-\infty}^{\infty} v_Y^2 P[v_Y] dv_Y \tag{7}$$

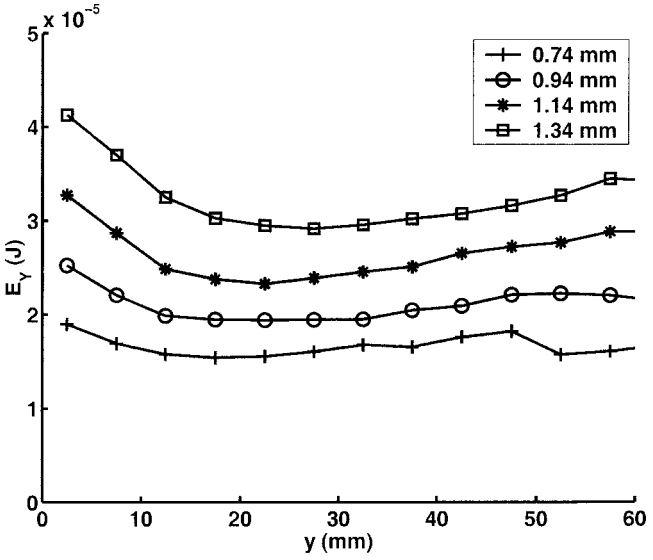

FIG. 7. Granular temperature profiles, resolved in the y direction, for $N = 1050$, and $A_O = 0.74$, 0.94, 1.14, and 1.34 mm.

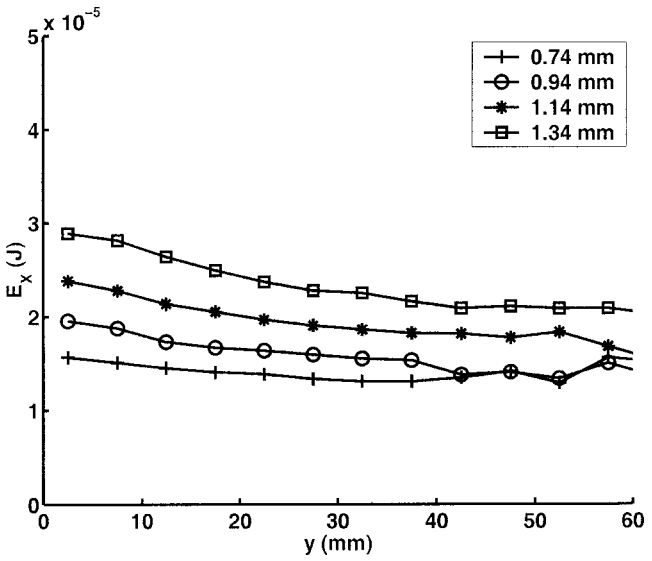

FIG. 8. Granular temperature profiles, resolved in the x direction, for $N=1050$, and $A_O=0.74$, 0.94, 1.14, and 1.34 mm.

leads to

$$E_Y = m\overline{v_Y'^2} + mv_C^2, \tag{8}$$

where v_Y' is the fluctuation velocity about the mean velocity.

At a height of 60 mm above the base, $v_C \sim 0.1\,\mathrm{m\,s^{-1}}$, indicating that one might expect an enhancement of $\sim 2\times10^{-6}$ J in the granular temperature. The measured difference between E_Y at $y=30$ mm and at $y=60$ mm is $\sim 6\times10^{-5}$ J, 30 times greater than might be expected from the above calculations, indicating that the upturn in granular temperature may not be ascribable to convection currents. Similar behavior has been seen in molecular dynamics (MD) studies [19] and is usually attributed to gradients in the concentration [20].

As expected, an increase in the amplitude of vibration tends to increase the granular temperature systematically at all heights. The scaling relationships involved between the granular temperature and the peak velocity are investigated in the next section.

IV. SCALING LAWS

A number of authors have attempted to relate the granular temperature or center-of-mass position to the base peak velocity. In two dimensions, Luding, Herrmann, and Blumen [21] used event-driven simulations to analyze the scaling of the height of the center-of-mass of a 2D fluidized granular bed. Similar results were observed in the experimental analysis of Warr, Huntley, and Jacques [5], in line with the simple kinetic theory of Huntley [22]. However, these results have all been at odds with other theoretical analyses [5,23] in describing the scaling exponents modeling the scaling between the peak base velocity and the number of grains, with the granular temperature or center-of-mass height. In three-dimensional systems the theoretical work of Kumaran [24] suggests that the scaling is expected to take a form similar to that proposed in Ref. [21], namely,

$$h_{\mathrm{c.m.}} - h_{\mathrm{c.m.},0} \approx (A_O\omega)^{\alpha}\left[\frac{n_b}{N(1-\varepsilon)}\right]^{\beta}, \tag{9}$$

where n_b is the average number of beads in a layer, $h_{\mathrm{c.m.}}$ is the height of the center of mass, and $h_{\mathrm{c.m.},0}$ is the height of the assembly of beads at rest. In 1D studies [16] α was found to take the value of 2, but in the 2D MD studies $\alpha=3/2$ [21]. Most theoretical models of similar systems suggest that $\alpha=2$ [5,24].

The scaling was investigated experimentally by three methods. First, by using the granular temperature profiles extracted from the short time mean squared displacement, and using an average of the scaling exponents measured at each height (Method 1); second, through the analysis of the behavior of the center-of-mass extracted from the packing fraction profiles (Method 2); and third, by fitting a Boltzmann packing profile to the experimental data at high altitude (Method 3). In the case of the granular temperature, only the y components were calculated; the scaling exponent was found to be variable for the x component. As stated earlier, the number of grains, N, was varied through $N=350$, 700, and 1050, while the amplitude of vibration A_O was 0.74, 0.94, 1.14, 1.34, and 1.54 mm. Not all these amplitudes were used for each value of N; the maximum amplitude before grains collided with the lid depended on the number of grains, and limited the vibration intensity. Figures 9(a) and 9(b) show the scaling relationships between E_Y and $A_O\omega$, and E_Y and n_b/N, respectively. Power law curves have been fitted to data sets, with resultant exponents α and β of 1.54 and 0.76, respectively. The scaling results are somewhat similar to the experimental and numerical results of Warr, Jacques, and Huntley [4] and Luding, Herrmann, and Blumen [21] respectively, but again, are significantly different from the theoretical predictions.

The second scaling analysis used the scaling of the center of mass to make a direct comparison with Luding, Herrmann, and Blumen [21]. The height of the center of mass was calculated by integrating the packing fraction profiles in Figs. 4(a) and 4(b) according to:

$$\langle y\rangle = \frac{\int y\,\eta(y)\,dy}{\int \eta(y)\,dy}. \tag{10}$$

The ground-state height of the grains was calculated using [21]

$$h_{\mathrm{c.m.},0} = \frac{n_b d}{2N}\left[(1-\sqrt{2/3})n_h + \sqrt{2/3}n_h^2\right] + \frac{n_0 d}{2N}\left[1+2\sqrt{2/3}n_h\right], \tag{11}$$

where n_h is the number of full layers and n_0 is the number of grains in the final layer. Figures 10(a) and 10(b) show the scaling of $h_{\mathrm{c.m.}} - h_{\mathrm{c.m.},0}$ with $A_O\omega$ and n_b/N. For the case of an isothermal system, following a Boltzmann distribution for the packing fraction as a function of height, the change in the center of mass is proportional to the temperature of the system. While these assumptions are not strictly valid here, the scaling exponents were nevertheless calculated, giving α and β values of 1.24 and 0.36, respectively. These scaling expo-

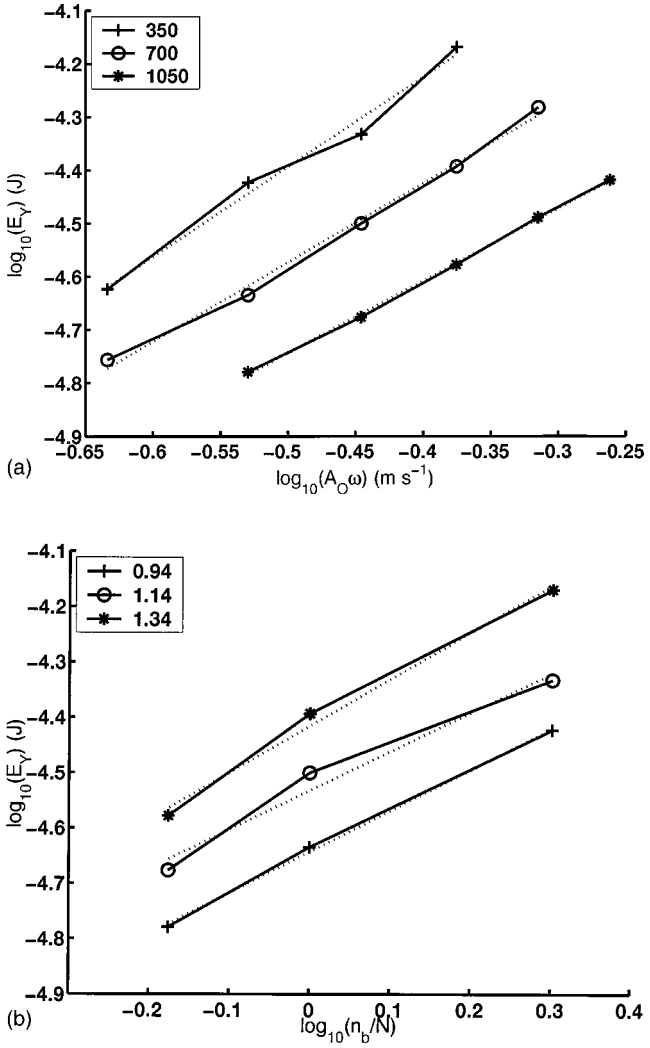

FIG. 9. Scaling relationships between $\log_{10}(E_Y)$ and (a) $\log_{10}(A_O\omega)$ for $N=350$, 700, and 1050 and (b) $\log_{10}(n_b/N)$ for $A_O=0.94$, 1.14, and 1.34 mm.

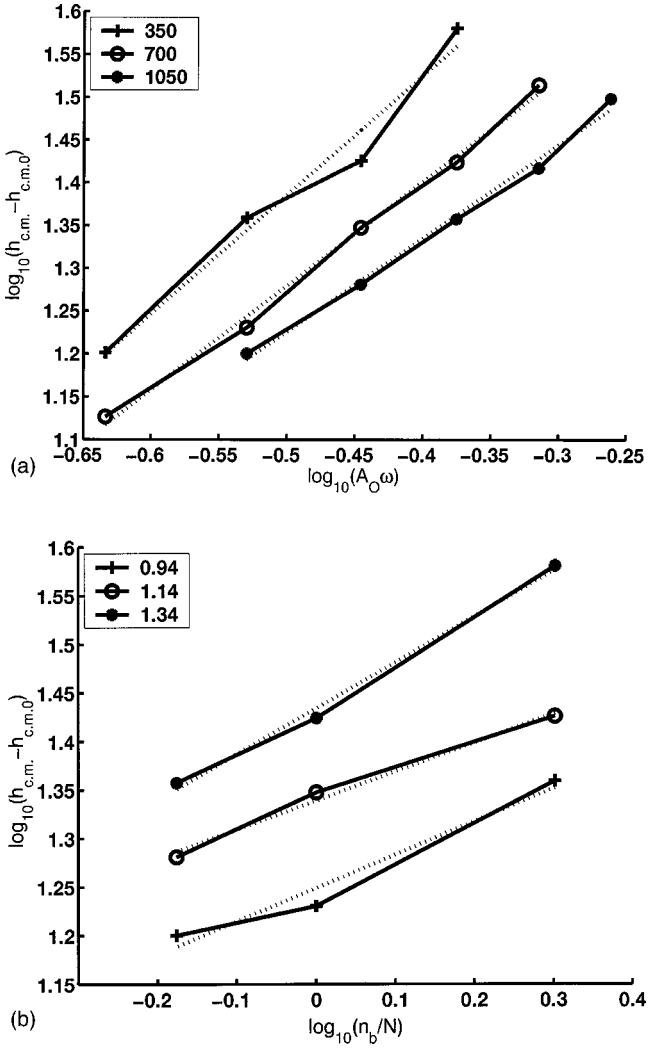

FIG. 10. Scaling relationships between $\log_{10}(h_{\text{c.m.}}-h_{\text{c.m.},0})$ and (a) $\log_{10}(A_O\omega)$ for $N=350$, 700, and 1050, and (b) $\log_{10}(n_b/N)$ for $A_O=0.94$, 1.14, and 1.34 mm.

nents differed significantly from those predicted from both theory and simulation (Table I), and also as might be expected, from the scaling exponents extracted from the granular temperature E_Y.

The third method of determining the scaling was to estimate the granular temperature by fitting an exponentially decaying Boltzmann density distribution to the high altitude packing fraction profiles. This analysis was performed for all datasets to enable the extraction of the relationship between E_O, N, and A_O, resulting in exponents of $\alpha=1.85\pm0.30$ and $\beta=0.76\pm0.13$.

The disparity between the theoretical predictions and the experiments may have its source in a number of factors. A suggestion of Warr, Huntley, and Jacques was that in 2D, the dissipation of energy during sliding collisions with the confining glass wall might result in a source of error [5]. Here in 3D, this effect is not present and may be dismissed as a source of error. The majority of theoretical explanations predict $\alpha=2$, apart from Huntley [22] who predicted ~1.4 for dense systems as opposed to the dilute system under investigation here, and Kumaran [24] who predicted $\alpha=1.5$ for situations in which drag dissipation was the dominant source of energy loss. The event-driven simulations of Luding, Herrmann, and Blumen [21] determined an exponent of 1.5, where of course the dissipation due to drag was zero. This suggests that the theoretical studies are missing a fundamental aspect of granular fluidization. Although air drag *was*

TABLE I. Comparison of the theoretical, numerical, and experimental results for the scaling exponents α and β.

Method	α	β
2D E_O scaling [5]	1.41 ± 0.03	0.6 ± 0.03
2D $h_{\text{c.m.}}-h_{\text{c.m.},0}$ [5]	1.3 ± 0.04	0.27 ± 0.11
Simulation [21]	1.5 ± 0.01	1.0
Theory [5,24]	2.0	1.0
Method 1: 3D E_O scaling	1.54 ± 0.37	0.76 ± 0.07
Method 2: 3D $h_{\text{c.m.}}-h_{\text{c.m.},0}$	1.24 ± 0.15	0.37 ± 0.09
Method 3: 3D E_O from η	1.85 ± 0.30	0.76 ± 0.13

present in our experiments, its relative importance compared to collisional dissipation can be quantified. Assuming no air currents, for particle speeds of about $\bar{c}\sim 1\ \mathrm{m\,s^{-1}}$, the Reynolds number Re is about 300, leading to an estimate of the drag coefficient, $C_d\sim 0.66$ [25]. The frictional drag force is then given by

$$F_d=\frac{C_d}{8}\pi\rho_f d^2\bar{c}^2, \tag{12}$$

where ρ_f is the fluid (air) density. This leads to a value of $\sim 7\times 10^{-6}\ \mathrm{N}$ for the drag force. For mean free paths, λ, of about 70 mm, this results in an approximate energy dissipation of $\sim 5\times 10^{-7}\ \mathrm{J}$ per collision period. The energy lost due to a collision can be estimated by [4,26]

$$\Delta E_c\approx \tfrac{1}{2}m\overline{c^2}(1-\varepsilon^2), \tag{13}$$

resulting in about $1.6\times 10^{-5}\ \mathrm{J}$ dissipated during a typical collision. Therefore the energy dissipated through drag forces is some 3% of the loss through collisions. This suggests that, to a first approximation, drag may be neglected, implying that for the system examined here, the explanation of Kumaran [24] is not applicable. The analytical models of the vibrofluidized system use an exponentially decaying packing profile with an isothermal atmosphere. Figures 4(a)–(d), 7, and 8 show that this is clearly not the case. Another potential source of the difference, grain-wall dissipation, is discussed in the following section.

V. SIDEWALL EFFECTS

The packing fraction profile in Fig. 4(d) shows a significant influence of the sidewalls on the system. Previous analytical studies by Kumaran [24] considered the effect of grain-grain dissipation and viscous drag but not the sidewalls; numerical studies of scaling exponents by McNamara [15] estimated the magnitude of the dissipation at the wall, but did not assess the impact on the scaling laws. Qualitatively, one observes that at the lowest excitation levels, most grains will interact almost exclusively with other grains or the base, but that as the base velocity is increased and the bed becomes more fluidized, collisions with the sidewalls will become progressively more likely. This additional loss mechanism can, therefore, be expected to reduce the scaling exponent α below the theoretical value of two.

In quantitative terms, the simple model described in Refs. [5] and [24], in which the steady state temperature is established by assuming Maxwell-Boltzmann statistics and equating rates of energy input and energy dissipation, can be extended relatively straightforwardly. The isothermal Boltzmann number density profile $n(y)$ (valid only for the lowest packing fractions, see e.g., Ref. [27])

$$n(y)=\frac{mgN}{A_C E_O}\exp\left(-\frac{mgy}{E_O}\right) \tag{14}$$

results in a total grain-grain dissipation rate

$$D_{gg}=4\sqrt{\pi}r^2\frac{N^2}{A_C}g(mE_O)^{1/2}(1-\varepsilon^2) \tag{15}$$

for three dimensions, where A_C is the cross-sectional area of the cell and r is the grain radius [24]. The leading-order term in the total energy input rate for a symmetrical driving signal is [24]

$$S_O=\frac{Nmg}{E_O}2\left(\frac{2}{\pi}\right)^{1/2}(mE_O)^{1/2}\langle V^2\rangle, \tag{16}$$

where V is the base velocity and

$$\langle V^2\rangle=\frac{V_O^2}{2} \tag{17}$$

for a sinusoidal wave form where V_O is the peak base velocity. The additional loss term due to grain-wall interactions can be obtained by assuming frictionless collisions (tangential motion of the wall therefore having no effect), characterized by a restitution coefficient ε_w. The total rate of dissipation through grain-wall contact was estimated by considering the energy lost during a collision,

$$\delta E=\frac{m}{2}(1-\varepsilon_w^2)v_X^2, \tag{18}$$

and the rate of collisions on an area $\pi d_c dy$ around the wall,

$$dR=\frac{1}{4\pi}n(y)\pi d_c\,dy\,cP(c)dc\int_0^{2\pi}d\phi\int_0^{\pi/2}\cos\theta\sin\theta\,d\theta, \tag{19}$$

where θ and ϕ are the polar angles of the velocity vector and $P[c]$ is the Maxwell distribution of speeds. Thus, the integration of the product of Eqs. (18) and (19) leads to the expression for the total rate of dissipation due to wall-grain collisions:

$$D_{gw}=\left(\frac{8}{\pi}\right)^{1/2}\frac{E_O^{3/2}}{m^{1/2}}(1-\varepsilon_w^2)\frac{N}{d_c}. \tag{20}$$

Under steady state conditions we expect

$$D_{gg}+D_{gw}=S_O, \tag{21}$$

which results in the following expression for granular temperature:

$$(1-\varepsilon_w^2)E_O^2+\frac{\sqrt{2}mgd_cNd^2\pi}{4A_C}(1-\varepsilon^2)E_O-m^2gd_c\langle V^2\rangle=0. \tag{22}$$

This reduces to the elastic wall case for $\varepsilon_w\to 1$.

Figure 11 shows the scaling dependence of E_O with V_O calculated for both the elastic and the inelastic wall cases for the range of experimental conditions prevailing in the present study. The value of ε_w was measured to be 0.68 ± 0.04 using high-speed photography. The scaling exponent resulting from the modified expression ranged from 1.27 to

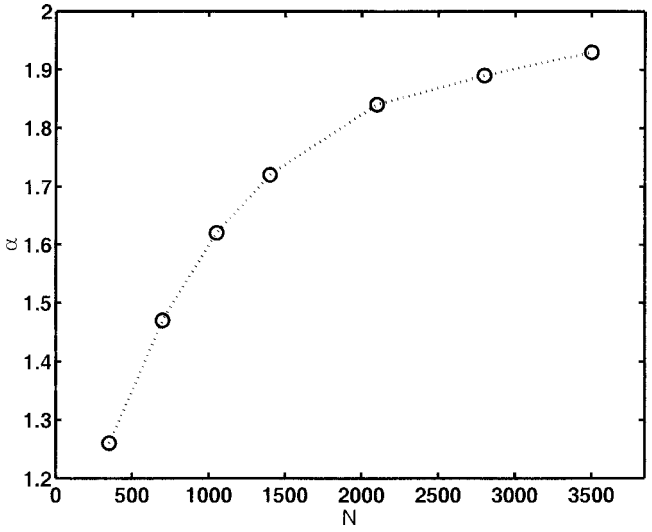

FIG. 11. The scaling exponent α, as defined by Eq. (9), for inelastic grain-wall collisions as a function of N through solution of Eq. (22).

1.75 as can be seen from Fig. 11, all lower than that calculated using the elastic wall case, but also showing a strong N dependence.

In summary, the analysis of the effects of the drag, intergrain, and the grain-wall dissipation indicates that the dominant loss terms are likely to be due to collisions. Previous investigations into the scaling of the granular temperature with the peak base velocity have tended to assume that the influence of the sidewalls is small. However, we have shown in this paper that wall effects can be quite large, not just in affecting the scaling but also the radial distribution of the packing fraction. This effect is N dependent, and is significant at low values of N. This can be understood in terms of the mean free path of the grains. At low packing fractions the mean free path may be of similar size to the dimensions of the experimental cell. As the packing fraction increases, the relative influence of the walls is reduced as the grains interact with each other more frequently and the expression for E_O returns to that for the case in which the side walls are neglected. The analysis described here shows that the walls can act as significant heat sinks, dissipating the kinetic energy of the system through grain-wall collisions, and any complete description of a granular bed must model this aspect of granular flow in three-dimensional geometries.

CONCLUSIONS

The fine temporal resolution and the long experimental times obtained by using positron emission particle tracking have allowed the state variables in a three-dimensional vibrofluidized granular bed to be characterized. Granular temperature profiles were determined for a range of N and A_O. Packing fraction was measured both as a function of y, but also as a function of the distance from the cylinder axis. This indicated that in regions close to the wall the packing fraction was enhanced. Determination of the velocity fields showed that convection rolls were present, but were typically less than 10% of the root mean squared fluctuation speed and their influence was small during measurement of the granular temperature. The scaling relationships between the granular temperature, the number of layers of grains and the base velocity in the y direction were broadly in line with results from two-dimensional studies. An explanation for the lower values of the scaling parameters was proposed. The dissipation of the kinetic energy of the grains through wall collisions was considered as an extra term in the steady state energy balance equation. Numerical analysis of the results showed that reduced scaling exponents would be expected for grain-wall restitution coefficients less than one.

ACKNOWLEDGMENTS

The work was funded by the Engineering and Physical Sciences Research Council under contract GR/L61781, and by Shell International Oil Products B.V. The authors would like to thank Professor Jean-Pierre Hansen for useful discussions and Mr. D. Britton for his invaluable technical assistance.

[1] H. M. Jaeger and S. R. Nagel, Phys. Today **49** (4), 32 (1996); H. M. Jaeger, S. R. Nagel, and R. P. Behringer, Rev. Mod. Phys. **68**, 1259 (1996).
[2] J. T. Jenkins and S. B. Savage, J. Fluid Mech. **130**, 187 (1983); A. Goldshtein and M. Shapiro, *ibid.* **282**, 75 (1995); J. T. Jenkins and M. W. Richman, Phys. Fluids **28**, 3485 (1985).
[3] C. S. Campbell, Annu. Rev. Fluid Mech. **22**, 57 (1990).
[4] S. Warr, G. T. H. Jacques, and J. M. Huntley, Powder Technol. **81**, 41 (1994).
[5] S. Warr, J. M. Huntley, and G. T. H. Jacques, Phys. Rev. E **52B**, 5583 (1995).
[6] S. Warr and J.-P. Hansen, Europhys. Lett. **36**, 589 (1996).
[7] R. D. Wildman and J. M. Huntley, Powder Technol. **113**, 14 (2000).
[8] R. D. Wildman, J. M. Huntley, and J.-P. Hansen, Phys. Rev. E **60**, 7066 (1999).
[9] N. Menon and D. J. Durian, Science **275**, 1920 (1997).
[10] E. E. Ehrichs, H. M. Jaeger, G. S. Karczmar, J. B. Knight, V. Y. Kuperman, and S. R. Nagel, Science **267**, 1632 (1995).
[11] D. J. Parker, D. A. Allen, D. M. Benton, P. Fowles, P. A. McNeil, M. Tan, and T. D. Beynon, Nucl. Instrum. Methods Phys. Res. A **392**, 421 (1997).
[12] R. D. Wildman, J. M. Huntley, J.-P. Hansen, D. J. Parker, and D. A. Allen, Phys. Rev. E **62**, 3826 (2000).
[13] D. J. Parker, A. E. Dijkstra, T. W. Martin, and J. P. K. Seville, Chem. Eng. Sci. **52**, 2011 (1997).
[14] R. D. Wildman, S. Blackburn, P. McNeil, P. Benton, and D. J. Parker, Powder Technol. **103**, 220 (1999).
[15] S. McNamara and S. Luding, Phys. Rev. E **58**, 2247 (1998).
[16] S. Luding, E. Clement, A. Blumen, J. Rajchenbach, and J. Duran, Phys. Rev. E **49**, 1634 (1993).
[17] J. R. Henderson and F. van Swol, Mol. Phys. **51**, 991 (1984).

[18] R. D. Wildman, J. M. Huntley, and D. J. Parker, Phys. Rev. Lett. **86**, 3304 (2001).
[19] K. Helal, T. Biben, and J.-P. Hansen, Physica A **240**, 361 (1997).
[20] R. Soto, M. Mareschal, and D. Risso, Phys. Rev. Lett. **83**, 5003 (1999).
[21] S. Luding, H. J. Herrmann, and A. Blumen, Phys. Rev. E **50**, 3100 (1994).
[22] J. M. Huntley, Phys. Rev. E **58**, 5168 (1998).
[23] V. Kumaran, J. Fluid Mech. **364**, 163 (1998).
[24] V. Kumaran, Phys. Rev. E **57**, 5660 (1998).
[25] J. P. K. Seville, U. Tüzün, and R. Clift, *Processing of Particulate Solids* (Blackie, London, 1997).
[26] T. G. Drake, J. Fluid Mech. **225**, 121 (1991).
[27] T. Biben, J.-P. Hansen, and J.-L. Barrat, J. Chem. Phys. **98**, 7330 (1993).